Photocatalytic degradation of an emerging pollutant by TiO$_2$-coated glass rings: a kinetic study

Agustina Manassero, María Lucila Satuf & Orlando Mario Alfano

Springer

CrossMark

AOPS: RECENT ADVANCES TO OVERCOME BARRIERS IN THE TREATMENT OF WATER, WASTEWATER AND AIR

Photocatalytic degradation of an emerging pollutant by TiO₂-coated glass rings: a kinetic study

Agustina Manassero[1] · **María Lucila Satuf**[1] · **Orlando Mario Alfano**[1]

Abstract This work presents the photocatalytic degradation of the pharmaceutical drug clofibric acid in a fixed-bed reactor filled with TiO₂-coated glass rings. Experiments were carried out under UV radiation. A kinetic model that takes into account radiation absorption by means of the local surface rate of photon absorption (LSRPA) has been developed. The LSRPA was obtained from the results of a radiation model. The Monte Carlo method was employed to solve the radiation model, where the interaction between photons and TiO₂-coated rings was considered. Data from experiments carried out with rings with different numbers of catalyst coatings and different irradiation levels were used to estimate the parameters of the kinetic model. A satisfactory agreement was obtained between model simulations and experimental results.

Keywords Photocatalysis · Kinetic model · Clofibric acid · Fixed-bed reactor · TiO₂-coated glass rings · Monte Carlo method

Introduction

Photocatalysis is an advanced oxidation technology with potential use in the degradation of a wide range of organic pollutants in the gas or liquid phase. Photocatalytic reactions start with the absorption of photons with energy larger than the band gap of the semiconductor catalyst. Then, electrons from the valence band are promoted to the conduction band, generating electron-hole pairs. These charge carriers can migrate to the surface of the catalyst and participate in reduction and oxidation reactions with the chemical species adsorbed, leading to the degradation of the pollutants. Among several catalysts, titanium dioxide (TiO₂) is one of the most used because it has high stability, good performance, and low cost (Moreira et al. 2011).

Photoreactors employed in heterogeneous photocatalysis can be grouped into two broad categories: reactors having TiO₂ particles in suspension (slurry reactors) and reactors with TiO₂ immobilized on different inert supports (fixed-film and fixed-bed reactors). Slurry reactors offer a high surface area for reactions, ensuring a shorter time for pollutant degradation compared to the reactors with immobilized TiO₂. However, reactors with suspended catalyst have several drawbacks that include particle aggregation at high photocatalyst concentration, the requirement of a filtration step after the photocatalytic treatment, and the impossibility to apply a continuous process (Vaiano et al. 2015). These limitations can be overcome by the use of films of TiO₂ immobilized on different supports, such as stainless steel, glass slides, beads, and Raschig rings (Sampaio et al. 2013).

For scale-up and design purposes of photocatalytic reactors, it is necessary to develop kinetic models that take into account the local rate of photon absorption. In this way, the kinetic parameters estimated from the fitting of the experimental data will be independent of shape and configuration of the reactor and, consequently, could be extrapolated to other reactor configurations. Therefore, a precise determination of the spatial distribution of the absorbed radiation should be accomplished. Among the different numerical methods for the calculation of the rate of photon absorption, the Monte Carlo (MC) method is preferred in reactors with complicated geometries (Moreira et al. 2010).

Springer

The aim of the present work is to simulate the photocatalytic degradation of a pharmaceutical in a fixed-bed reactor. Glass rings have been selected as support for the TiO_2 films because they have a large surface area and relatively high light transmittances, which benefit the radiation distribution inside the reactor (Cloteaux et al. 2014). Clofibric acid (CA), a pharmaceutical employed as blood lipid regulator, has been chosen as the model pollutant. The photocatalytic degradation of CA in slurry reactors has already been demonstrated, reaction intermediates have been identified, and degradation pathways have been proposed (Doll and Frimmel 2004; 2005 and Li et al., 2011). However, to the best of our knowledge, a kinetic model on the degradation of this pharmaceutical in a fixed-bed reactor has not yet been published.

The rate of photon absorption was obtained by using the Monte Carlo method. Subsequently, these results were incorporated in a kinetic model to compute the theoretical evolution of CA concentration and its main intermediate, 4-chlorophenol (4-CP). An optimization algorithm was used to estimate the kinetic parameters by comparing the model predictions with the experimental results obtained in the laboratory reactor.

Materials and methods

Experimental device

Experiments were carried out in a fixed-bed reactor filled with 5×5 mm borosilicate glass rings coated with TiO_2. The wall thickness of the rings was 0.75 mm. The reactor was cylindrical, made of glass, with a volume of 54 cm^3. A total of 310 rings were employed to fill the reactor, in random dispositions. The aqueous solution was introduced into the reactor through two inlet ports at the bottom of the reactor and exited from a single exit port situated on top. The inlet ports are placed obliquely creating a swirl-flow of the liquid inside the reactor, ensuring a well-mixed solution. It was irradiated from one side through a circular flat window with a halogenated mercury lamp (Powerstar HQI-TS 150W/NDL from OSRAM) placed at the focal axis of a parabolic reflector. The illuminated window was made of borosilicate ground glass. The lamp has an emission spectrum ranging from 350–550 nm. To irradiate the reactor only with UV radiation, a container with a solution of $CoSO_4$ was interposed between the reactor and the lamp. The resulting spectral distribution of radiation that reaches the reactor window is shown in Fig. 1. In order to modify the irradiation level, two optical neutral filters were used to provide transmittances of 62 and 30 % of the total radiation. These filters attenuate the incident radiation without altering the spectral distribution of the lamp. They were constructed on polyester sheets transparent to UV-A radiation and were printed with different tones of gray, with the aid of commercial
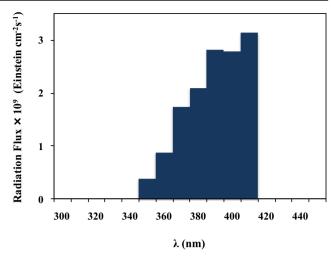

Fig. 1 Spectral distribution of radiation that reaches the reactor window

software, to provide the different transmission levels. Figure 2 shows a schematic representation of the fixed-bed reactor.

The reactor is part of a recycling system that includes a peristaltic pump (Masterflex) and a storage tank of 1000 cm^3 equipped with a device for withdrawing of samples, a thermometer, and a gas inlet for oxygen supply. The isothermal condition (25 °C) was achieved by the incorporation of a water-circulating jacket to the storage tank. A schematic representation of the experimental device can be found in Manassero et al. (2015).

Experimental runs were carried out by varying the number of coatings on the glass rings (1, 3, and 5) and the incident radiation levels reaching the reactor window (30, 62, and 100 %).

The incident radiation fluxes at the reactor window, experimentally measured by ferrioxalate actinometry (Murov et al. 1993), were 15.2, 9.39, and 4.58 nEinstein s^{-1} cm^{-2} for 100, 62, and 30 %, respectively.
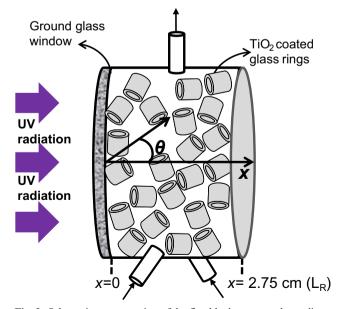

Fig. 2 Schematic representation of the fixed-bed reactor and coordinate system

Immobilization of TiO_2

The catalyst was immobilized on the glass rings by the dip-coating technique employing a suspension of 150 g L^{-1} of TiO_2 (TiO_2 Aeroxide P25, Evonik Degussa GmbH, Germany). The rings were dipped into the suspension at room temperature and extracted at a constant withdrawal speed of 3 cm min^{-1} (van Grieken et al. 2009). Afterward, the rings were dried at 110 °C for 24 h and calcined at 500 °C for 2 h with a heating rate of 5 °C min^{-1}. This procedure was repeated to produce rings with different numbers of TiO_2 coatings.

A spectrophotometric technique (Jackson et al. 1991) was employed to quantify the mass of TiO_2 immobilized per square centimeter of rings. This technique involves the acidic digestion of the catalyst fixed on the glass support followed by the addition of H_2O_2 to form a colored complex that is photometrically detected at 410 nm. The mass of catalyst immobilized was 0.02, 0.05, and 0.08 mg cm^{-2} for 1, 3, and 5 coatings, respectively.

In order to estimate the thickness of the films immobilized over the rings, glass plates were coated with TiO_2 employing the same suspension and procedure as for the rings. The thickness of these films was calculated from SEM images acquired by a scanning electron microscope (JEOL, JSM-35C) equipped with an acquisition system of digital images (SemAfore). The average thicknesses were 0.11, 0.27, and 0.44 μm for 1, 3, and 5 coatings, respectively.

Photocatalytic experiments

The solution to be treated was prepared by adding 20 mg of CA in a 1000-mL volumetric flask and diluting to volume with ultrapure water. Before starting each experimental run, the reactor was filled up with the coated rings and the solution was placed in the tank. Then, the pump was switched on and the solution was circulated in the system for 60 min in order to reach the adsorption equilibrium between CA and the TiO_2 coatings. In the meantime, the solution was fed with oxygen and the lamp was turned on in order to stabilize the photon emission. During this time, the lamp was shielded with a shutter to prevent the arrival of radiation to the reactor. Once the system was stabilized and the adsorption equilibrium was reached, the first sample was taken from the tank and the shutter was removed to start the reaction. Samples were taken every 120 min for a total period of 660 min. The initial concentration of CA in all experiments was 9.30×10^{-8} mol cm^{-3}.

Samples were analyzed by HPLC with a UV detector to measure CA and 4-CP concentrations (Waters chromatograph provided with a RP C-18 column XTerra®). The mobile phase was a binary mixture of acidified water (with 0.1 % v/v phosphoric acid) and acetonitrile (50:50). Absorbance detection was made at 227 nm (Dordio et al. 2009).

Experiments at pH 2, pH 5 (natural pH), and pH 10 were performed in order to determine the best condition for the photocatalytic assays. The highest CA conversion was obtained at pH 5 and, therefore, natural pH has been selected as the initial condition.

Additionally, a control experiment was carried out in the reactor without coated rings in order to evaluate the direct photolysis of the pollutant under the irradiation conditions employed in this study. No significant changes were detected in the concentration of CA after 300 min of irradiation.

Mass balances

The assumptions made to obtain the mass balances for CA and 4-CP in the reaction system were the following: (i) the conversion per pass in the reactor is differential, (ii) the system is well-mixed, (iii) mass transfer limitations are negligible, (iv) direct photolysis is insignificant, and (v) chemical reactions occur only at the solid-liquid interface among adsorbed molecules. Thus, the general form of the mass balance in the reacting system for a generic compound i can be written as follows (Satuf et al. 2007):

$$\frac{dC_i}{dt} = \frac{A_{cat}}{V_T} \langle r_i(x,t) \rangle_{A_{cat}} \qquad (1)$$

where C_i is the molar concentration of i (mol cm^{-3}), t refers to the reaction time (s), V_T is the total volume (cm^3), and $\langle r_i(x,t) \rangle_{A_{cat}}$ represents the surface degradation rate of the i compound averaged over the catalytic area, A_{cat} (cm^2).

The simplified reaction pathway for the photocatalytic degradation of CA considers the degradation of CA to generate the organic intermediate 4-CP. Next, the degradation of 4-CP leads to the formation of secondary organic intermediates (X_i). Finally, these intermediate compounds could be eventually mineralized to HCl, CO_2, and H_2O (Fig. 3). Other possible oxidation products like 4-chlorocatechol, hydroquinone and benzoquinone were not considered in the kinetic modeling because their concentrations never reached significant levels. In this way, the resulting mass balances for CA and 4-CP with the corresponding initial conditions, are as follows:

$$\frac{dC_{CA}}{dt} = -\frac{A_{cat}}{V_T} \langle r_{CA},(x,t) \rangle_{A_{cat}} \qquad C_{CA}(t=0) = C_{CA,0} \quad (2)$$

$$\frac{dC_{4-CP}}{dt} = \frac{A_{cat}}{V_T} \left[\langle r_{CA},(x,t) \rangle_{A_{cat}} - \langle r_{4-CP},(x,t) \rangle_{A_{cat}} \right] \qquad C_{4-CP}(t=0) = 0$$
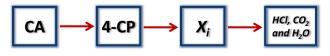
$$(3)$$

Fig. 3 Reaction pathway for CA degradation

Kinetic model

The reaction scheme proposed for the photocatalytic degradation of CA is shown in Table 1 (Turchi and Ollis 1990; Almquist and Biswas 2001).

The reaction rate expressions were obtained based on the above scheme and taking into account the following assumptions: (i) photocatalytic reactions occur at the surface of the catalyst particles among adsorbed molecules (Pelizzetti and Minero 1993); (ii) dynamic equilibrium is achieved between the bulk and the adsorbed concentrations of H_2O, O_2, inorganic species, and organic compounds (Almquist and Biswas 2001; Dijkstra et al. 2002); (iii) molecular oxygen and organic compounds are adsorbed on different sites of the catalyst (Turchi and Ollis 1990; Terzian et al. 1990); (iv) competitive adsorption between CA and its main reaction intermediates is postulated; (v) the attack by the hydroxyl radical is the main degradation mechanism for CA and its intermediates (Mills and Davies 1993; Theurich et al. 1996); (vi) O_2 concentration is constant and in excess with respect to the stoichiometric demand (Satuf et al. 2007); (vii) the concentration of water molecules and hydroxyl ions on the catalytic surface remains constant (Satuf et al. 2007); and (viii) the superficial concentration of total adsorption sites for CA, per unit area of catalyst, can be considered constant. Also, the low values of the Thiele modulus (Φ) and the optical thickness (τ) obtained for the thickest film (i.e., the most unfavorable condition, $\Phi_{5\text{coatings}} = 1.90 \times 10^{-4}$ and $\tau_{5\text{coatings}} = 0.062$) allow us to assume that inside the TiO_2 film, the concentration of CA and the local volumetric rate of photon absorption are almost uniform (Camera-Roda and Santarelli 2007). From these assumptions, the following reaction rate expressions were obtained:

$$r_{CA} = \frac{\alpha_2 C_{CA}(t)}{1 + \alpha_3 C_{CA}(t) + \alpha_5 C_{4-CP}(t)} \left(-1 + \sqrt{1 + \alpha_1 e^{a,s}(x)}\right) \tag{4}$$

$$r_{4-CP} = \frac{\alpha_4 C_{4-CP}(t)}{1 + \alpha_3 C_{CA}(t) + \alpha_5 C_{4-CP}(t)} \left(-1 + \sqrt{1 + \alpha_1 e^{a,s}(x)}\right) \tag{5}$$

where α_i are intrinsic kinetic parameters, and $e^{a,s}$ is the local surface rate of photon absorption (LSRPA); that is, the amount

Table 1 Reaction scheme for the photocatalytic degradation of CA

Step	Reaction	Reaction rate
Activation	$TiO_2 + h\nu \rightarrow e^- + h^+$	r_{gs}
Recombination	$e^- + h^+ \rightarrow$ heat	$k_2[e^-][h^+]$
Electron trapping	$e^- + O_{2,ads} \rightarrow \cdot O_2^-$	$k_3[e^-][O_{2,ads}]$
Hole trapping	$h^+ + H_2O_{ads} \rightarrow \cdot OH + H^+$	$k_4[h^+][H_2O_{ads}]$
	$h^+ + OH^-_{ads} \rightarrow \cdot OH$	
Hydroxyl attack	$CA_{ads} + \cdot OH \rightarrow \rightarrow 4-CP$	$K_5[CA_{ads}][\cdot OH]$
	$4-CP_{ads} + \cdot OH \rightarrow X_i$	$k_6[4-CP_{ads}][\cdot OH]$

of photons absorbed per unit time and per unit area of the TiO_2-coated surface. A detailed derivation of these equations can be found in Manassero et al. (2015).

Local surface rate of photon absorption

As observed in Eqs. (4) and (5), it is necessary to evaluate the $e^{a,s}$ by the TiO_2 films. In this work, the Monte Carlo (MC) method has been applied to obtain $e^{a,s}$ at each point in the fixed-bed reactor. This method consists of tracking the trajectory of a great number of photon bundles and computing the locations where they are absorbed. The trajectories and fates of these photons are determined by using randomly generated numbers (R_i) between 0 and 1.

Due to the fact that radiation extinction by the coated rings occurs mainly along the longitudinal axis of the cylindrical reactor, and considering the incoming diffuse radiation at the reactor window, the radiation can be modeled with one spatial variable (x) and one angular variable (θ). The coordinate system employed in the radiation model is shown in Fig. 2.

The 1D radiation model considers that photons travel with a linear trajectory in the aqueous phase until they reach a ring wall or the reactor walls. Those photons that reach the rings can be absorbed by the TiO_2 film, reflected or transmitted. The absorbed photons are stored in a spatial cell, the trajectory ends and a new photon bundle is considered. On the other hand, if the photons are reflected, the new direction is determined by considering specular reflection (Imoberdorf et al. 2007). Those photons that are transmitted through the ring may interact with other rings, until they are absorbed or they reach the reactor walls. It is important to note that the radiation absorption by the glass rings was not taken into account because the absorption of the borosilicate glass is negligible in the range of the lamp emission. A flowchart of the MC algorithm developed is shown in Fig. 4.

The spectral distribution of the incident radiation was discretized into eight wavelengths. Also, the reactor length was divided into small cells of length Δx to store the position of the absorbed photons. Briefly, the model considers the following events:

Event 1: Photon direction. The ground glass window ensures diffuse radiation at the inner side of the reactor window; therefore, the same probability is assigned to all directions (Spadoni et al. 1977) and the angle θ that determines the direction of the photons is given by:
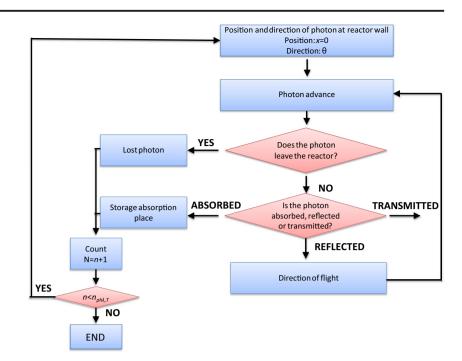
$$\theta = asin(2R_1 - 1) \tag{6}$$

Event 2: Length of the photon flight. The distance that photons can travel without reaching a ring (ξ), is determined by the mean free path of photons inside the reactor (*MFP*) and by a random number (R_2), according to (Imoberdorf et al. 2010):

$$\xi = -MFP\ln(R_2) \tag{7}$$

Fig. 4 Monte Carlo algorithm developed to evaluate the surface photon absorption rate in the fixed-bed reactor

The *MFP* was estimated as $MFP = V_R/A_{proj}$, where V_R is the reactor volume and A_{proj} is the total sum of the projected area of the rings ($A_{proj} = N_{rings} \times l \times d$, where N_{rings} is the number of rings in the reactor, and l and d are the length and diameter of an individual ring). The calculated value of *MFP* was 0.43 cm. Then, the new position of the photon bundle was determined as follows:

$$x_{new} = x_{old} + e_x\xi \tag{8}$$

where x_{old} refers to the previous location of the photon bundle inside the reactor, x_{new} refers to the new location, and e_x is the direction cosine.

Event 3: Reflection of the photons. A new random number (R_3) and the reflectivity (ρ) on the ring wall (calculated using the Fresnel equation) were used to evaluate the reflection of photons:

$$\begin{aligned} \rho > R_3 &\rightarrow \textit{The photons are reflected} \\ \rho < R_3 &\rightarrow \textit{The photons are absorbed or transmitted} \end{aligned} \tag{9}$$

Event 4: Absorption or transmission of the photons. If the photons are not reflected, the effective transmittance (T) was employed to evaluate if the photons are absorbed. T was estimated by the following equation (Vella et al. 2010):

$$T_{TiO_2\ coating} = exp(-\kappa_\lambda t_{TiO_2}) \tag{10}$$

where κ_λ is the spectral volumetric absorption coefficient of the TiO$_2$ film and t_{TiO_2} is the average thickness of the coatings. Values of κ_λ for each wavelength were obtained according to Marugán et al. 2015.

By using a new random number, R_4, it is possible to determine if the photon bundle is absorbed or transmitted, according to

$$\begin{aligned} T > R_4 &\rightarrow \textit{The photons are transmitted} \\ T < R_4 &\rightarrow \textit{The photons are absorbed} \end{aligned} \tag{11}$$

If photons are transmitted, the length of the photon flight is estimated with Eq. (7) and the sequence continues. If photons are absorbed, the absorption position is stored and the trajectory ends.

Finally, the LSRPA in each cell of the reactor was calculated as

$$e^{a,s}(x) = \sum_\lambda \frac{q_{w\lambda} n_{ph\lambda,abs}(x) V_R}{n_{ph\lambda,T} \Delta x A_{cat}} \tag{12}$$
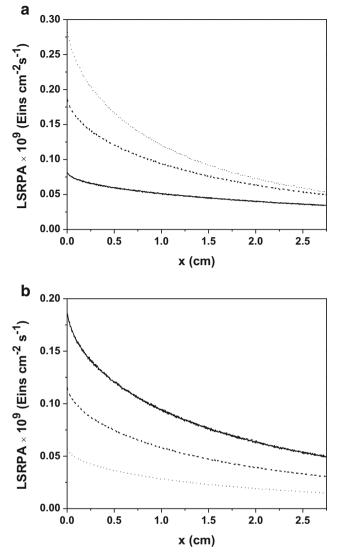
where $q_{w\lambda}$ is the radiation flux of wavelength λ incident at the reactor window, $n_{ph\lambda,abs}$ represents the number of photons of wavelength λ absorbed in a cell of position x and length Δx, and $n_{ph\lambda,T}$ is the total number of the photons of wavelength λ considered in the simulation. The value of $q_{w\lambda}$ was calculated from the spectral distribution of the radiation that reaches the reactor and from the polychromatic radiation flux.

The simulation involved the tracking of 10^8 photon bundles for each wavelength.

Results and discussion

Profiles of local surface rate of photon absorption

The profiles of the absorbed radiation in the fixed-bed reactor, obtained with Monte Carlo simulations, for different

a

b

Fig. 5 LSRPA profiles in the reactor. *a* Rings with different numbers of TiO$_2$ coatings and 100 % irradiation level: one coating (*solid line*), three coatings (*broken line*), and five coatings (*dotted line*). *b* Rings with three coatings and different levels of irradiation: 100 % of irradiation (*solid line*), 62 % of irradiation (*broken line*), and 30 % of irradiation (*dotted line*)

numbers of TiO$_2$ coatings and different levels of irradiation, are shown in Fig. 5. As observed in Fig. 5 (a), the LSRPA increases with the number of TiO$_2$ coatings. This difference is more significant near the reactor window ($x = 0$), while the LSRPA acquires practically the same values at $x = L_R$. Also, as expected, the LSRPA decreases as the irradiation level is attenuated (Fig. 5 (b)).

It is worth noting that the profiles of radiation absorption estimated for this fixed-bed reactor are smoother than those estimated for a slurry reactor of the same dimensions (Manassero et al. 2015). In the reactor filled with TiO$_2$-coated rings, the LSRPA decreases when we move away from the irradiated window, but it never reaches zero. This situation indicates the absence of dark zones in the reactor, leading to a better utilization of its volume.

Estimation of kinetic parameters

The predicted values of CA and 4-CP concentrations were obtained by introducing the kinetic expressions (Eqs. 4 and 5) into the mass balances:

$$\frac{dC_{CA}}{dt} = -\frac{A_{cat}}{V_T}\langle r_{CA}\rangle A_{cat} = -\frac{A_{cat}}{V_T}\left(\frac{\alpha_2 C_{CA}}{1+\alpha_3 C_{CA}+\alpha_5 C_{4-CP}}\right) \tag{13}$$
$$\left\langle -1+\sqrt{-1+\alpha_1 e^{a,s}(x)}\right\rangle_{A_{cat}} C_{CA}(t=0)=C_{CA,0}$$

$$\frac{dC_{4-CP}}{dt} = \frac{A_{cat}}{V_T}\langle r_{4-CP}\rangle A_{cat} = \frac{A_{cat}}{V_T}\left(\frac{\alpha_2 C_{CA}-\alpha_4 C_{4-CP}}{1+\alpha_3 C_{CA}+\alpha_5 C_{4-CP}}\right) \tag{14}$$
$$\left\langle -1+\sqrt{-1+\alpha_1 e^{a,s}(x)}\right\rangle_{A_{cat}} C_{4-CP}(t=0)=0$$

To obtain the five parameters involved in the kinetic expressions, the Levenberg-Marquardt optimization method was used. This optimization algorithm minimizes the sum of the square of the differences between predicted and experimental concentrations.

Table 2 Kinetic parameters of both complete and simplified model

	Parameter	Value	95 % confidence interval	Units
Five-parameter model	α_1	1.27×10^{10}	0.20×10^{10}	cm^2 s Einstein^{-1}
	α_2	6.38×10^{-5}	0.48×10^{-5}	cm s^{-1}
	α_3	2.67×10^{-5}	0.16×10^{-5}	cm^3 mol^{-1}
	α_4	5.12×10^{-4}	0.72×10^{-4}	cm s^{-1}
	α_5	1.01×10^{-6}	0.34×10^{-6}	cm^3 mol^{-1}
Three-parameter model	α_1	2.95×10^{10}	0.31×10^{10}	cm^2 s Einstein^{-1}
	α_2	3.24×10^{-5}	0.11×10^{-5}	cm s^{-1}
	α_4	2.57×10^{-4}	0.25×10^{-4}	cm s^{-1}

Once the values of the kinetic parameters were obtained, it was possible to conclude that

$$\alpha_3 C_{CA} \ll 1 \text{ and } \alpha_5 C_{4-CP} \ll 1$$

Thus, the kinetic model can be simplified according to the following equations:

$$\frac{dC_{CA}}{dt} = -\frac{A_{cat}}{V_T}\alpha_2 C_{CA}\left\langle -1 + \sqrt{-1 + \alpha_1 e^{a,s}(x)} \right\rangle_{A_{cat}} \quad (15)$$

$$\frac{dC_{4-CP}}{dt} = \frac{A_{cat}}{V_T}(\alpha_2 C_{CA} - \alpha_4 C_{4-CP})\left\langle -1 + \sqrt{-1 + \alpha_1 e^{a,s}(x)} \right\rangle_{A_{cat}} \quad (16)$$

Therefore, a new estimation was carried out considering the simplified equations. The values of the kinetic parameters for the complete and simplified models are shown in Table 2.

Simulated and experimental concentrations of CA and 4-CP using glass rings with different numbers of TiO$_2$ coatings and 100 % irradiation level are shown in Fig. 6.

The initial reaction rate was accelerated when the number of catalyst coatings was increased from one to three (from 1.09×10^{-11} to 2.50×10^{-11} mol cm^{-3} s^{-1}). However, from three to five coatings, the reaction rate was only slightly increased (from 2.50×10^{-11} to 2.81×10^{-11} mol cm^{-3} s^{-1}). Therefore, experiments under different irradiation levels were carried out with rings containing three coatings of TiO$_2$.
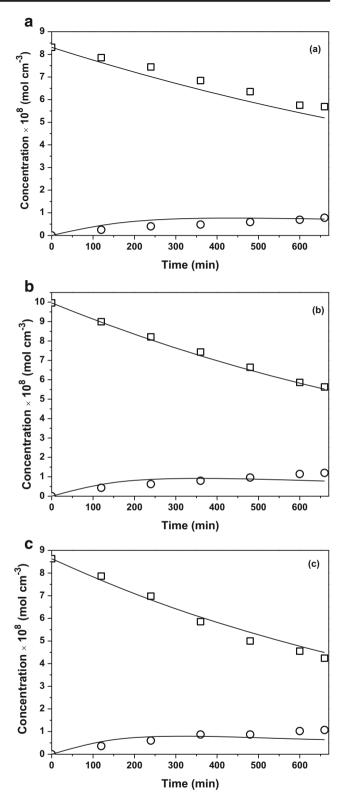
The initial reaction rate was 7.78×10^{-12}, 2.20×10^{-11}, and 2.50×10^{-11} mol cm^{-3} s^{-1} for 30, 62, and 100 % irradiation level, respectively. As expected, the reaction rate increases with the irradiation level, but the difference between the rate obtained with 62 % and the one obtained with 100 % is not very important. This effect can be attributed to the undesired increase in the recombination of the photogenerated electrons and holes in the catalyst at high levels of irradiation, reducing the availability of charge carriers to generate hydroxyl radicals.

The kinetic model could adequately simulate the degradation of CA and 4-CP under different experimental conditions. The root mean square error of the estimations, considering the concentrations of CA and 4-CP, was 14.7 %.

In order to assess the loss of activity of the catalytic films, four experiments were performed by reusing the glass rings with three TiO$_2$ coatings (each one involving 360 min of reaction). No significant differences in the final conversion of CA were obtained, showing that no appreciable loss of activity was found after 4 cycles of use of the catalytic rings.

Conclusions

In this work, the kinetic model of a photocatalytic, fixed-bed reactor filled with TiO$_2$-coated glass rings has been developed. The local rate of photon absorption, which was

Fig. 6 Photocatalytic degradation of CA using glass rings with different numbers of TiO$_2$ coatings. Symbols: experimental concentrations (*white square* = CA; *white circle* = 4-CP); *solid lines*: model simulations. **a** One coating, **b** three coatings, and **c** five coatings

necessary to evaluate the reaction rate of the model pollutant CA, was calculated by using Monte Carlo simulations. The

results obtained in this study show that the fixed-bed reactor can successfully degrade CA in aqueous solution. The TiO$_2$-coated glass rings, employed as filling, allow a deep penetration of radiation along the reactor, leading to a more efficient use of the incident photons when compared with slurry reactors. Moreover, the catalytic films supported on the glass rings are stable and show no deactivation after several reaction cycles, being readily applicable for continuous process.

With only three kinetic parameters, it was possible to estimate the concentration of CA and its main intermediate, 4-CP, under six different experimental conditions (three irradiation levels and three different numbers of TiO$_2$ coatings over the glass rings).

A_{cat}, catalytic area (cm^2); A_{proj}, projected area of the rings (cm^2); C, molar concentration (mol cm^{-3}); CA, clofibric acid; 4-CP, 4-chlorophenol; d, ring diameter (cm); $e^{a,s}$, local surface rate of photon absorption (Einstein cm^{-2} s^{-1}); e_x, direction cosine (dimensionless); l, ring length (cm); L_R, reactor length (cm); $LSRPA$, local surface rate of photon absorption (Einstein cm^{-2} s^{-1}); MC, Monte Carlo; MFP, mean free path (cm); N_{rings}, number of rings in the reactor; n_{ph}, number of photons; q_w, incident radiation flux (nEinstein s^{-1} cm^{-2}); R_i, random number; r, surface degradation rate (mol cm^{-2} s^{-1}); T, effective transmittance (dimensionless); t_{TiO_2}, average thickness of the coatings (cm or μm); t, time (s); V, volume (cm^3); X_i, secondary organic intermediates; x, axial coordinate (cm); **x,** position vector (cm)

Greek letters

α_i, α_i', kinetic parameter; κ, spectral volumetric absorption coefficient (cm^{-1}); ξ, length of flight (cm); ρ, Reflectivity (dimensionless); θ, spherical coordinate (rad)

Subscripts

abs, Absorbed; CA, clofibric acid; 4-CP, 4-chlorophenol; λ, dependence on wavelength; R, Reactor; T, Total; Tk, Tank; 0, initial condition

Special symbols

$\langle\rangle$, denotes average value over a given space; Δx, length of the cells employed in MC simulations (cm)

References

Almquist CB, Biswas P (2001) A mechanistic approach to modeling the effect of dissolved oxygen in photo-oxidation reactions on titanium dioxide in aqueous systems. Chem Eng Sci 56:3421–3430

Camera-Roda G, Santarelli F (2007) Optimization of the thickness of a photocatalytic film on the basis of the effectiveness factor. Catal Today 129:161–168

Cloteaux A, Gérardin F, Thomas D, Midoux N, André JC (2014) Fixed bed photocatalytic reactor for formaldehyde degradation: experimental and modeling study. Chem Eng J 249:121–129

Dijkstra MFJ, Panneman HJ, Winkelman JGM (2002) Modeling the photocatalytic degradation of formic acid in a reactor with immobilized catalyst. Chem Eng Sci 57:4895–4907

Doll T, Frimmel F (2004) Kinetic study of photocatalytic degradation of carbamazepine, clofibric acid, iomeprol and iopromide assisted by different TiO$_2$ materials-determination of intermediates and reaction pathways. Water Res 38:955–964

Doll T, Frimmel F (2005) Photocatalytic degradation of carbamazepine, clofibric acid and iomeprol with P25 and Hombikat UV100 in the presence of natural organic matter (NOM) and other organic water constituents. Water Res 39:403–411

Dordio A, Estêvão Candeias A, Pinto A, Teixeira da Costa C, Palace Carvalho A (2009) Preliminary media screening for application in the removal of clofibric acid, carbamazepine and ibuprofen by SSF-constructed wetlands. Ecol Eng 35:290–302

Imoberdorf GE, Alfano OM, Cassano AE, Irazoqui HA (2007) Monte Carlo model of UV-radiation interaction with TiO$_2$-coated spheres. AIChE J 53:2688–2703

Imoberdorf GE, Vella G, Sclafani A, Rizzuti L, Alfano OM, Cassano AE (2010) Radiation model of a TiO$_2$-coated, quartz wool, packed-bed photocatalytic reactor. AiChE J 56:1030–1044

Jackson NB, Wang CM, Luo Z, Schwitzgebel J, Ekerdt JG, Brock JR, Heller A (1991) Attachment of TiO$_2$ powders to hollow glass microbeads. Activity of the TiO$_2$- coated beads in the photoassisted oxidation of ethanol to acetaldehyde. J Electrochem Soc 138:3660–3664

Li W, Lu S, Qiu Z, Lin K (2011) Photocatalysis of clofibric acid under solar light in summer and winter seasons. Ind Eng Chem Res 50:5384–5393

Manassero A, Satuf ML, Alfano MO (2015) Kinetic modeling of the photocatalytic degradation of clofibric acid in a slurry reactor. Environ Sci Pollut Res 22:926–937

Marugán J, van Grieken R, Pablos C, Satuf ML, Cassano AE, Alfano OM (2015) Photocatalytic inactivation of *Escherichia coli* aqueous suspensions in a fixed-bed reactor. Catal Today 252:143–149

Mills A, Davies R (1993) Photomineralisation of 4-chlorophenol sensitised by titanium dioxide: a study of the intermediates. J Photochem Photobiol A 70:183–191

Moreira J, Serrano B, Ortíz A, de Lasa H (2010) Evaluation of photon absorption in an aqueous TiO$_2$ slurry reactor using Monte Carlo simulations and macroscopic balance. Ind Eng Chem Res 49:10524–10534

Moreira J, Serrano B, Ortíz A, de Lasa H (2011) TiO$_2$ absorption and scattering coefficients using Monte Carlo method and macroscopic balances in a photo-CREC unit. Chem Eng Sci 66:5813–5821

Murov SL, Carmichael I, Hug GL (1993) Handbook of photochemistry. Marcel Dekker, New York

Pelizzetti E, Minero C (1993) Electrochim Acta 38:47

Sampaio MJ, Silva CG, Silva AMT, Vilar VJP, Boaventura RAR, Faria JL (2013) Photocatalytic activity of TiO$_2$-coated glass raschig rings on the degradation of phenolic derivatives under simulated solar light irradiation. Chem Eng J 224:32–38

Satuf ML, Brandi RJ, Cassano AE, Alfano OM (2007) Quantum efficiencies of 4-chlorophenol photocatalytic degradation and mineralization in a well-mixed slurry reactor. Ind Eng Chem Res 46:43–51

Spadoni G, Bandini E, Santarelli F (1977) Scattering effects in photosensitized reactions. Chem Eng Sci 33:517–524

Terzian R, Serpone N, Minero C, Pelizzetti E, Hidaka H (1990) Kinetic studies in heterogeneous photocatalysis 4. The photomineralization of a hydroquinone and a catechol. J Photochem Photobiol A 55:243–249

Theurich J, Lindner M, Bahnemann DW (1996) Photocatalytic degradation of 4-chlorophenol in aerated aqueous titanium dioxide suspensions: a kinetic and mechanistic study. Langmuir 12:6368–6376

Turchi CS, Ollis DF (1990) Photocatalytic degradation of organic water contaminants: mechanisms involving hydroxyl radical attack. J Catal 122:178–190

Vaiano V, Sacco O, Pisano D, Sannino D, Ciambelli P (2015) From the design to the development of a continuous fixed bed photoreactor for photocatalytic degradation of organic pollutants in wastewater. Chem Eng Sci 137:152–160

van Grieken R, Marugán J, Sordo C, Pablos C (2009) Comparison of the photocatalytic disinfection of E. coli suspensions in slurry, wall and fixed-bed reactors. Catal Today 144:48–54

Vella G, Imoberdorf GE, Sclafani A, Cassano AE, Alfano OM, Rizzuti L (2010) Modeling of a TiO2-coated quartz wool packed bed photocatalytic reactor. Appl Catal B-Environ 96: 399–407